Proceedings of the 21st ICSMGE, Vienna, Austria, 14 – 19 June 2026. Pistrol, Adam & Schweiger (eds.)
Published by: ÖGG, Austrian Society for Geomechanics, Salzburg, Austria, ISBN 978-3-9503898-4-5
https://doi.org/10.53243/ICSMGE2026-1956

On the role of boundary conditions in the simulation of large deformation rockfall barriers

Marco Previtali, **Matteo Ciantia**
School of Science and Engineering, University of Dundee, United Kingdom; m.previtali5b@gmail.com

ABSTRACT: In recent years, the advances in computational power have enabled the explicit simulation of each individual components of rockfall barriers. However, this approach remains thus far constrained to structures with a relatively low number of elements. For stochastic or sensitivity analyses, where computational efficiency is crucial, a multi-scale approach is generally preferred. Within this context, the Discrete Element Method (DEM) offers efficient modelling of interactions among a large number of bodies but sacrifices some representativeness, particularly in the way structural elements such as fence posts and selvedge cables are implemented as boundary conditions. In this study, a recently developed macroelement model for double-twisted mesh is used to simulate the response of a mesh panel loaded using a circular platter. The structural elements, i.e. fence posts, are modelled using a combination of fixity conditions applied to discrete elements and coupling with continuum elements. A parametric analysis is then conducted to identify the effect of the boundary conditions. This analysis aims to quantify how the underlying assumptions affect the failure state of the barrier in the scope of reliability analysis for the mitigation of natural hazards.

KEYWORDS: Large deformation barrier, Steel wire mesh, Coupled DEM-FDM, Reliability analysis.

1 INTRODUCTION

Flexible protection barriers are perhaps the most widely used passive mitigation system for natural hazards such as rockfalls, debris flows and snow avalanches. In recent years, numerical methods have become a staple technique to assess their response to complex loading conditions beyond what is feasibly done with experimental tests. However, the simulation of such structures is characterized by several challenges: (i) large displacements, (ii) non-linear material and geometrical interactions and (iii) dynamic behaviour, that can be difficult to model using standard continuum techniques. The Discrete Element Method (DEM) has the advantage of fulfilling all these "advanced" numerical requirements within its basic formulation, while also providing a suitable framework to simulate multi-body natural hazards such as debris flows (Albaba et al., 2017). However, this approach can end up sacrificing the representation of the structural elements of the barrier, which are easier to define in a continuum (Finite Element Method, FEM) environment (e.g. Escallón et al., 2015). For this reason, various methods were proposed to integrate structural features in DEM (e.g. Effeindzourou et al., 2015; Coulibay et al., 2019). Still, their implementation can be challenging, especially in commercial codes that offer limited customization options. Quantifying the effect of these simplifications is therefore useful to assess the barrier performance when more accurate formulations are not available. Herein, the effect of modelling the fence posts as a deformable object is compared to the common assumption of fixity at the mesh edges (e.g. Tahmasbi et al., 2019; Li et al., 2018; Previtali et al., 2021b; Pol et al., 2021), by coupling DEM meshes with Finite Differences (FDM) fence posts.

2 MODEL DEFINITION

2.1 *Test setup*

The model geometry is constituted by a square mesh with a side length L of 3 meters, displaced in the out-of-plane (x) direction by a semi-spheroidal platter of diameter D, for a distance X of 0.5 meters. To reduce the number of parameters, the mesh is loaded under quasi-static conditions and no gravity. The edges of the mesh are intertwined to a selvedge wire (displacement continuity), which is then connected to the base and head of the fence posts, as shown in Figure 1b. The effect of the boundary conditions is investigated by (i) changing the platter diameter and keeping the panel size constant and (ii) changing the cross-section bending stiffness of the fence posts and keeping the mesh stiffness constant. In the latter, the limit scenario of infinitely rigid beams corresponds to the standard practice of fixing the velocities of the DEM particles at the edges of the mesh. Regarding the parametric study of the beam stiffness, the fence post geometries tested in Buzzi et al., (2013), were selected as reference to provide reasonable values, as summarised in Table 1 (R1-3) and Figure 1a. Four auxiliary (A1-4) beam geometries were also tested to expand the parameter space investigated. Six platter sizes are tested, with D/L ranging from 1/12th to 2/3rd, representing a behaviour ranging from mesh puncturing (e.g. individual rock fragments) to large, distributed loads (e.g. debris flows) for a total of 8 x 6 = 48 simulations.

2.2 *Numerical framework*

The mesh panels and selvedge wires are simulated within the DEM framework through the standard approach of defining remote bonds between discrete particles (Figure 2a), while the fence posts are modelled using hexahedral elements in a FDM environment. The commercial codes PFC3D and FLAC3D are here respectively used for each domain. The two interact through volumetric coupling (Figure 2b): given a number of DEM particles located within a FDM element, two weighting functions (w_{DEM}, w_{FDM}) are used to interpolate the influence of each numerical method on the kinematic variables (e.g. the velocity $\boldsymbol{v}$), so that their sum equals one at every point in the overlap area (Figure 2a). Lagrange multipliers are then used to enforce the continuity between DEM particles and FDM grid points (Breugnot et al., 2016; Cheng et al., 2023). The DEM mesh is obtained by placing the discrete elements according to the wire pattern and defining a series of remote contact interactions. The DT mesh employs and hexagonal pattern and a user-defined elasto-plastic model, previously calibrated on large-displacement FEM simulations and laboratory tests. Model details and calibration parameters are available in Previtali et al., (2026). For the scope of this paper, suffice to say that individual wires reach quasi-perfect plasticity at a load of 5 kN. Since the model directly prescribes forces and moments at the wire extremities, only two particles are used to discretize each wire piece. The selvedge cable is modelled using the parallel bond model, which implement slender Euler beam behaviour (Previtali et al., 2021a). Since it is a strand rope and not circular-section beam, plastic deformation and bending stiffness are considered negligible and an equivalent elastic

stiffness of 120 GPa and 16 mm diameter is used to match the tensile response. Finally, the von Mises model is used to simulate the fence posts within the FDM domain, considering a standard S355 steel, with a Young's modulus of 210 GPa, yield strength of 355 MPa and plastic hardening modulus of 2 GPa.

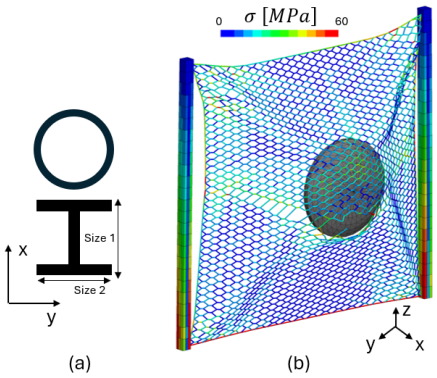

Figure 1. Model setup: (a) fence posts cross-section area, (b) geometry of the test. The DT pattern is parallel to the y direction, therefore $K_1 = K_y$ and $K_2 = K_z$.

Table 1. Sizes (mm) and Bending stiffness (EI, N/mm^2) of the fence posts cross-section. The first three cases are from Buzzi et al. (2013).

Id	Geometry	Size 1	Size 2	Wall Thickness	EI
R1	H	160	150	8	0.47
R2	Annulus	133	133	4.5	0.79
R3	Annulus	165	165	5	1.69
A1	Annulus	100	100	5	0.35
A2	Annulus	150	150	5	1.26
A3	Annulus	180	180	7.5	3.18
A4	Annulus	250	250	10	11.42
F	Fixed	N/A	N/A	N/A	Infinite

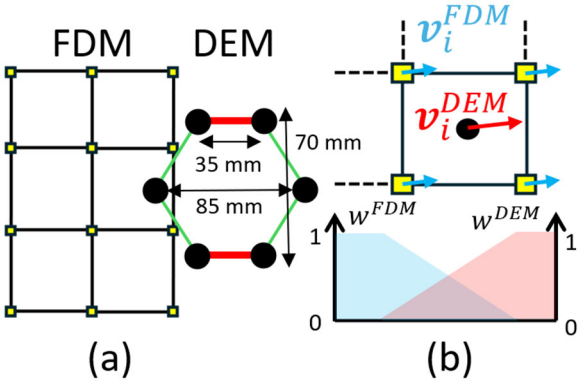

Figure 2: (a) discretization of fence posts and the steel meshes within FDM and DEM frameworks; (b) schematic of the volumetric coupling adopted.

For comparison's sake, the mesh and fence post stiffness can be reduced to a single stiffness (kN/m) scalar parameter, so that their ratio K_r can be used to quantify the way barrier displacement is subdivided between the mesh wires and the structural components. Regarding the fence posts, this single value can be identified by assuming negligible axial deformation (EA ≫ EI) and treating them as rollers connected to horizontal springs (Figure 3b). From cantilever beam theory, $K_{post} = 3EI/L^3$, which produces values from 39 to 1260 kN/m. The mechanical response of the mesh is too complex to be obtained analytically, but it can be measured and assumptions can be made to obtain a single value: since the sides of the mesh are free to rotate, no out-of-plane bending occurs during the test and the overall response is equivalent to that of a membrane with anisotropic in-plane stiffness. As the barrier is loaded in its centre, tension is concentrated within the diagonal direction (Timoshenko & Woinowsky, 1959). Using membrane theory and assuming negligible Poisson's effect on shear stiffness, the equivalent stiffness in this direction (θ) is obtained as:

$$\frac{1}{K_{eq}} = \frac{\cos^4\theta}{K_1} + \frac{\sin^4\theta}{K_2} + \frac{\sin^2\theta\cos^2\theta}{K_{shear}} \quad (1)$$

Where θ is here set to 45 degrees due to the square mesh shape, $K_{1,2}$ are the axial stiffnesses in the two planar directions and K_{shear} is the shear stiffness. This single parameter (K_{eq}) is here considered sufficient to characterise the mesh stiffness: the upper quadrant of the mesh and the selvedge are under minimal tension as the load is concentrated in the diagonal (Figure 1b) and the mesh relaxes due to the fence post deflection (Figure 3a). The lower quadrant is under significant tensile stress, but the fence post stiffness has no influence: the lower corners of the mesh are de-facto pinned, since they are connected to the base of the fence post instead of a more realistic combination of uphill anchor and mid-point connection to the fence posts. Finally, the lateral deflection of the mesh boundary is governed by the constant horizontal mesh stiffness (K_1) against the variable fence post stiffness: the selvedge cable itself has no effect since it has negligible bending stiffness and the fence posts are considered axially stiff.

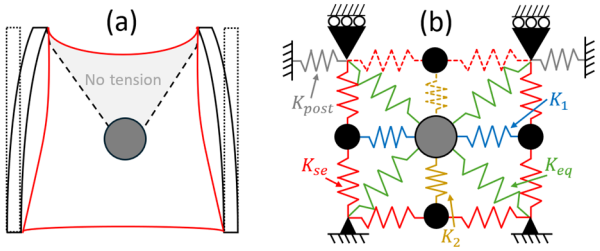

Figure 3. Definition of the analytical model: (a) simplified response as deformed mesh and horizontally deflected fence posts, (b) analytical representation of the model as a combination of springs. The springs in the upper quadrant are shown with dashed lines to indicate they are inactive.

The mesh stiffness in the different directions is here characterised using in-plane constant width tensile and rail shear tests (Figure 4). The directions for K_1 and K_2 are set as parallel and orthogonal to the orientation of the mesh pattern.

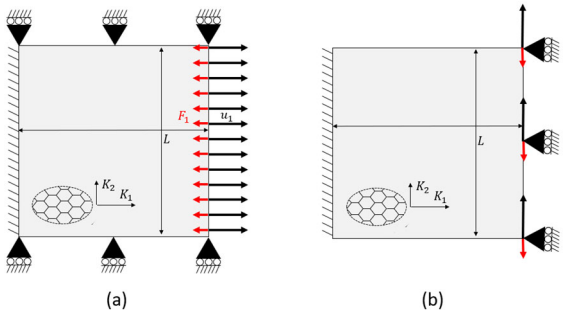

Figure 4. Schematics for (a) tensile and (b) shear tests.

3 RESULTS AND DISCUSSION

3.1 *Mesh stiffness*

The meso-scale properties of the mesh are obtained from the DEM simulations, by applying a controlled displacement rate and measuring the reaction force: the axial and shear stiffness is obtained as $K = F/u$ within the linear portion of the curve, normalised by mesh width L. This is repeated in both the directions parallel and orthogonal to the mesh pattern to retrieve the two stiffness values, i.e. $K_{1,2}$, resulting in values of 3.88 and 4.45 MPa, respectively (Figure 5). The same is done for the shear test, resulting in a stiffness of 51.08 kPa. The mesh stiffness value is obtained using eq. 1 and setting a length of 0.3 m as the width of the mesh portion under diagonal loading, producing a K_{mesh} of 15 kN/m. This value of 0.3 is chosen somewhat arbitrarily after observing the simulation results to provide a single conversion value, as the width of the tensile band changes slightly between the tests.

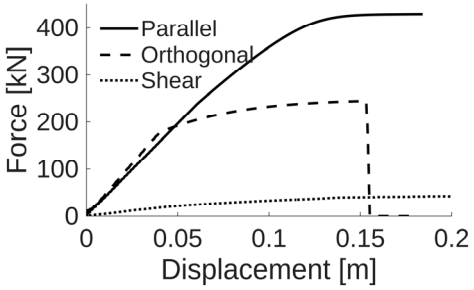

Figure 5. Force-displacement curves for the axial and shear pull tests.

3.2 *Punch test results*

Figure 6 and 7 show the force-displacement curves measured for the least (A1, $K_r = 2.59$) and most (F, K_r = Inf) stiff boundary conditions. In all scenarios, the initial portion of the curve ($X < 0.2$ m) is linear and broadly independent of the platter diameter. Afterwards, the reaction force increases non-linearly until a threshold, where the response become perfectly plastic. Both the degree of non-linearity and plasticity threshold depend on the platter diameter. Figure 8 shows the reaction force acting on the platter at the end of the simulation, normalised by the platter diameter (F/D). The case with the smallest diameter (D/L = 1/12) consistently produces the lowest F/D values, due to the onset of the bullet effect / localised plasticity. For the other scenarios, the normalised force (F/D) actually decreases with platter diameter. The rate of decay is inversely proportional to K_r, with barriers connected to stiff beams becoming less sensitive to increases in D/L. In the limit case (infinite stiffness), this effect almost disappears. Another thing to note is that the D/L value associated to the peak F/D increases with K_r, i.e. stiffer beams increase the platter diameter at which F/D is the highest.

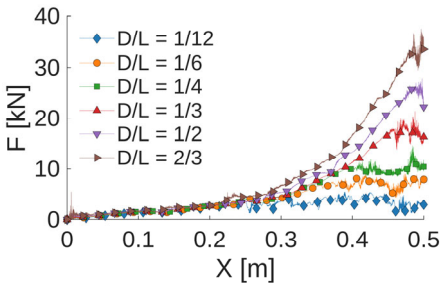

Figure 6. Force-displacement curves for the pinned edges, F scenario.

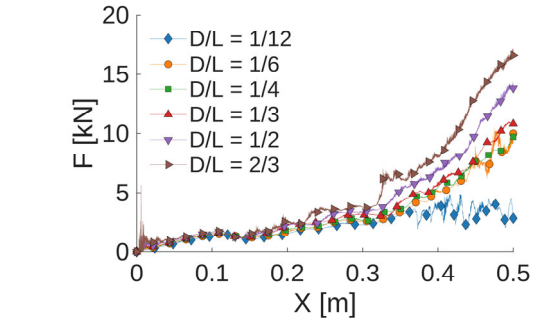

Figure 7. Force-displacement curves for the A1 scenario.

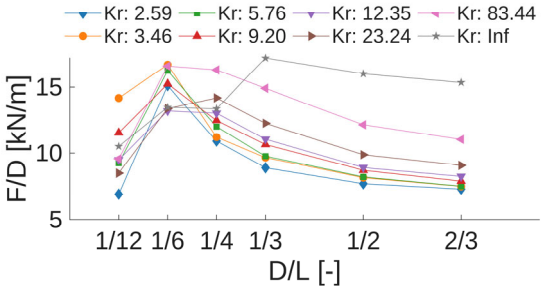

Figure 8. Reaction force acting on the platter at the end of the simulation, normalised by platter diameter.

Figures 9, 10 and 11 show the force-chain distribution at the end of the test for the scenarios A1-D1/6, A1-D2/3 and T-D1/6, respectively. The first one corresponds to the scenario characterised by peak F/D and high compliance beams: the tensile force is distributed in a wedge-like shape due to the mesh pattern. The force propagates from the centre following the single-wire orientation (Previtali et al., 2025) until it reaches the edges of the barrier, where it propagates to the edge along the double-twists. The upper quadrant is under no tension, as assumed in the theoretical model (Figure 3a). The out-of-plane displacement follows the standard cross-shaped distribution, i.e. it is concentrated along the diagonals.

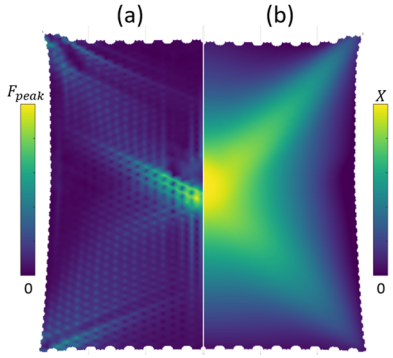

Figure 9. Distribution of (a) tension in the wires and (b) out of plane mesh displacement in the A1, D/L = 1/6 scenario.

In the second case (Figure 10), the forces are distributed across the entire domain and the mesh pattern has limited influence (i.e. it does not control the force propagation). This leads to the development of areas of tension in the bottom of the domain. A larger portion of the mesh is displaced, with additional areas of out-of-plane displacement, distinct from the one occurring at the diagonals. Finally, in the pinned-edges case (F), the force chain distribution is symmetric with respect to the vertical and it is concentrates along two bands at the side of the diagonal. Most of the tension is propagated across the single-wire orientation in proximity of the platter.

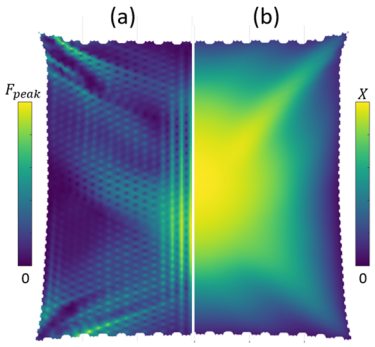

Figure 10. Distribution of (a) tension in the wires and (b) out of plane mesh displacement in the A1, D/L = 2/3 scenario.

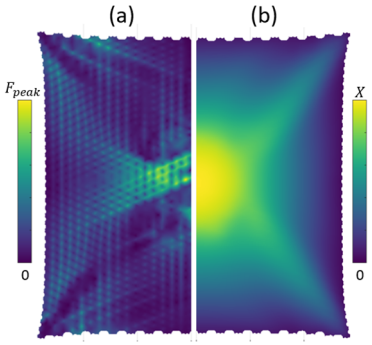

Figure 11. Distribution of (a) tension in the wires and (b) out of plane mesh displacement in the F, D/L = 1/3 scenario.

The data is interpreted as follows: during the test, the tensile force-chains developing at the platter interface first reach the edges of the mesh and then propagate to the corners, concentrating in a thin band (e.g. the mesh corners in Figure 9). The width and shape of the affected area (i.e. the tensile band) is governed by the pattern of the mesh and the resulting stiffness anisotropy, and not the size of the platter. Under these initial conditions, (e.g. $X < 0.2$ m, Figure 6), the stiffness of the response is therefore constant and depends only on the number of wires loaded near the mesh corner. As platter displacement continues, the force chains cannot propagate directly to the corner due to the discrete mesh pattern (e.g. Figure 10a) and additional force chains develop, connecting the edges of the platter to the selvedge. This increases the number of load bearing wires, producing the non-linear increase in the reaction force acting on the platter. Finally, the average tension in the band reaches the limit force of the constitutive model for a given wire ($F_{peak} \approx 5$kN) and perfectly plastic behaviour takes over at the barrier scale.

The maximum force acting on the platter therefore depends on the opposing influences of (i) the platter diameter and (ii) the fence post compliance. Under the hypothesis that the stiffness of the response depends on the transmission of force-chains onto the selvedge, increasing the platter diameter allows for more wires (outside the diagonal) to bear the load, while increasing the beam compliance collapses the load onto the diagonal, counteracting this effect.

4 CONCLUSIONS

A coupled DEM-FDM model was used to investigate the effect of fence post stiffness on the mesh response. The mesh response can be represented using a in-series spring model where the .fence-post spring is obtained from cantilever beam theory. The spring that represents the mesh is obtained from the stiffness anisotropy of the mesh, assuming that the tensile force is concentrated along the mesh diagonal, as it is typically done for membranes.

Analysis of the simulation results showed that the latter assumption is necessarily true and the mesh does not behave as a membrane at all scales. Even for a relatively fine mesh sieve size, if the tensile band is not aligned with the orientation of the individual wires, the force chains propagate in discontinuous wedges. In this case, the fence post stiffness does not simply affect the overall stiffness of the system, but also affects the orientation of the force chains and therefore lowers the maximum force that can be withstood by the barrier.

5 REFERENCES

Albaba, A., Lambert, S., Kneib, F., Chareyre, B., & Nicot, F. (2017). DEM modeling of a flexible barrier impacted by a dry granular flow. *Rock Mechanics and Rock Engineering*, *50*, 3029-3048.

Breugnot, A., Lambert, S., Villard, P., & Gotteland, P. (2016). A discrete/continuous coupled approach for modeling impacts on cellular geostructures. *Rock Mechanics and Rock Engineering*, 49(5), 1831-1848.

Buzzi, O., Spadari, M., Giacomini, A., Fityus, S., & Sloan, S. W. (2013). Experimental testing of rockfall barriers designed for the low range of impact energy. *Rock mechanics and rock engineering*, 46(4), 701-712.

Cheng, H., Thornton, A. R., Luding, S., Hazel, A. L., & Weinhart, T. (2023). Concurrent multi-scale modeling of granular materials: Role of coarse-graining in FEM-DEM coupling. *Computer Methods in Applied Mechanics and Engineering*, 403, 115651.

Coulibaly, J. B., Chanut, M. A., Lambert, S., & Nicot, F. (2018). Sliding cable modeling: An attempt at a unified formulation. International *Journal of Solids and Structures*, 130, 1-10.

Coulibaly, J. B., Chanut, M. A., Lambert, S., & Nicot, F. (2019). Toward a generic computational approach for flexible rockfall barrier modeling. *Rock Mechanics and Rock Engineering*, *52*(11), 4475-4496.

Effeindzourou, A., Thoeni, K., Chareyre, B., & Giacomini, A. (2015). A general method for modelling deformable structures in DEM. In *PARTICLES IV: proceedings of the IV International Conference on Particle-Based Methods: fundamentals and applications* (pp. 744-754). CIMNE.

Escallón, J. P., Wendeler, C., Chatzi, E., & Bartelt, P. (2015). Mechanics of chain-link wire nets with loose connections. Engineering Structures, 101, 68-87.

Li, X., & Zhao, J. (2018). A unified CFD-DEM approach for modeling of debris flow impacts on flexible barriers. *International Journal for Numerical and Analytical Methods in Geomechanics*, 42(14), 1643-1670.

Previtali, M., Ciantia, M. O., Spadea, S., Castellanza, R., & Crosta, G. (2021a). Discrete element modeling of compound rockfall fence nets. In *International Conference of the International Association for Computer Methods and Advances in Geomechanics.* Cham: Springer International Publishing.

Previtali, M., Ciantia, M. O., Spadea, S., Castellanza, R. P., & Crosta, G. B. (2021b). Multiscale modelling of dynamic impact on highly deformable compound rockfall fence nets. *Proceedings of the Institution of Civil Engineers-Geotechnical Engineering*, 174(5), 498-511.

Previtali, M., Ciantia, M., Crosta, G. (2026). A novel constitutive model for double-twisted hexagonal meshes within the Macroelement framework. *Computer and Geotechnics*. 190, 107673.

Pol, A., Gabrieli, F., & Brezzi, L. (2021). Discrete element analysis of the punching behaviour of a secured drapery system: from laboratory characterization to idealized in situ conditions. *Acta Geotechnica*, 16(8), 2553-2573.

Tahmasbi, S., Giacomini, A., Wendeler, C., & Buzzi, O. (2019). On the computational efficiency of the hybrid approach in numerical simulation of rockall flexible chain-link mesh. *Rock Mechanics and Rock Engineering*, 52, 3849-3866.